Supplementary information

Inconsistency of Poisson-Boltzmann equation

As shown in Refs. [1, 2] the results of Poisson-Boltzmann equation contradict the superposition principle of electrostatics (potentials due to individual ions can be linearly superimposed to yield the potential due to an assembly of ions) which originates from the linear Poisson equation. The problems are remedied in the Debye-Hückel approximation $e^{\pm\psi} \approx 1 \pm \psi$, i.e. for small ψ. There is however no mathematical inconsistency in combining it with the non-linear Boltzmann equation as otherwise no sensible solution would be obtained[1].

The deeper reason of the inconsistency is the identification of the mean potential appearing in Poisson's equation (potential not changed by a spy-particle) with the potential of mean force appearing in the electrochemical potential and thus in the Boltzmann expression (potential referring to the distribution that self-consistently includes the particle). The inconsistency is also revealed by the fact that the Debye and the Güntelberg charging processes lead to different results. The differences disappear at low potentials since here interactions are negligible. The differences between both types of potentials may also become less relevant at very high field as here the contribution of the particle is expected to be less relevant according to Ref. [9].

As the Taylor expansion of the Poisson-Boltzmann equation shows, the validity of the exponential solution extends to greater ψ for symmetrical electrolytes as here the quadratic terms cancel.

More accurate descriptions of concentrated electrolytes are given by Mayer et al.[3], and Allnatt et al.[4-6], but may become soon very intransparent and not manageable. For more details the reader is referred to literature[1-11].

1. Onsager, L., Theories of Concentrated Electrolytes. *Chemical Reviews* **1933,** *13* (1), 73-89.
2. Casimir, H., Tweede Symposium over sterke Elektrolyten en de Elektrische Dubbellaag. *by Sectie voor Kolloid-chemie, Ned. Chem. Ver. Utrecht* **1944**, 1.
3. Mayer, J.; Mayer, M., Statistical Mechanics, John Wiley, New York **1940**.
4. Allnatt, A. R.; Lidiard, A. B., Atomic transport in solids, Cambridge University Press, Cambridge, **1993**.
5. Allnatt, A.; Loftus, E., Physical cluster theory of point defect interactions. II. Application to AgCl doped with CdCl2. *The Journal of Chemical Physics* **1973,** *59* (5), 2550-2559.

6. Allnatt, A.; Loftus, E., Erratum: Physical cluster theory of point defect interactions. II. Application to AgCl doped with CdCl2. *The Journal of Chemical Physics* **1979,** *71* (12), 5388-5388.

7. Münster, A., Statistical thermodynamics II, chapter 18, Springer, **1974**.

8. Bockris, J. O. M.; Reddy, A. K., Modern Electrochemistry 1. Plenum Press, New York **1977**.

9. Lyklema, J., Fundamentals of interface and colloid science, Volume I, Fundamentals, chapter 4.3 c, Academic press, London, **1991**.

10. Lyklema, J., Fundamentals of interface and colloid science, Volume II, Solid-liquid interfaces, chapter 3.6 a, Academic press, London, **2001**.

11. Conway, B., Physical Chemistry: An Advanced Treatise. Vol. IXA,"Electrochemistry," H. Eyring, Ed., Academic Press, New York, **1970**.

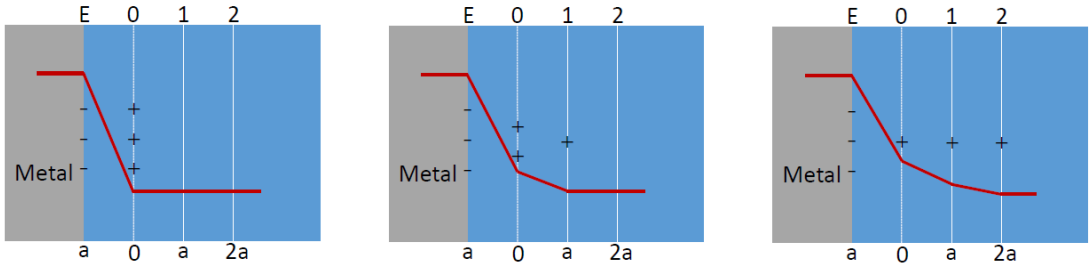

$$\frac{\mathcal{L}}{a} = \frac{0 \times 3}{3} = 0$$

$$\frac{1}{C_{tot}} = \frac{\partial(\phi_E - \phi_0)}{\partial Q} = \frac{a}{\varepsilon}$$

$$\frac{\mathcal{L}}{a} = \frac{0 \times 2 + 1 \times 1}{3} = \frac{1}{3}$$

$$\frac{1}{C_{tot}} = \frac{\partial(\phi_E - \phi_0)}{\partial Q} + \frac{\partial(\phi_0 - \phi_1)}{\partial Q} = \frac{a}{\varepsilon} + \frac{a}{3\varepsilon}$$

$$\frac{\mathcal{L}}{a} = \frac{0 \times 1 + 1 \times 1 + 2 \times 1}{3} = 1$$

$$\frac{1}{C_{tot}} = \frac{\partial(\phi_E - \phi_0)}{\partial Q} + \frac{\partial(\phi_0 - \phi_1)}{\partial Q} + \frac{\partial(\phi_1 - \phi_2)}{\partial Q} = \frac{a}{\varepsilon} + \frac{a}{\varepsilon}$$

Figure S1. A few simple situations for centroid calculations.

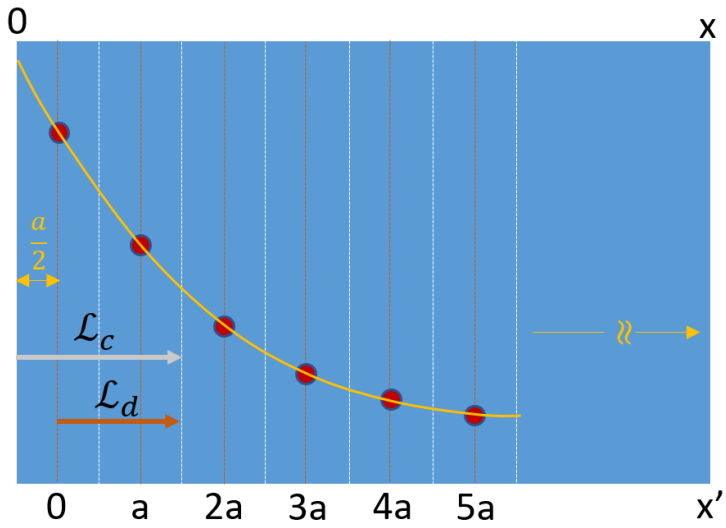

Figure S2. Sketch of centroid in continuous model and discrete model.

When various linear charge profiles are investigated, $\mathcal{L}_{discrete} + \frac{a}{2} = \mathcal{L}_{continuous}$ is exactly fulfilled for the horizontal curve, while the difference becomes slightly less for finite slopes. A deviation from $\frac{a}{2}$ means that the absolute position of the centroid deviate slightly. Obviously when $\mathcal{L} \to 0$, the absolute centroid position will tend toward $\frac{a}{2}$ and the difference tend to zero. The horizontal example shows that the smearing out on the rhs is without influence. The deviations cannot be consistently investigated with linear solutions.

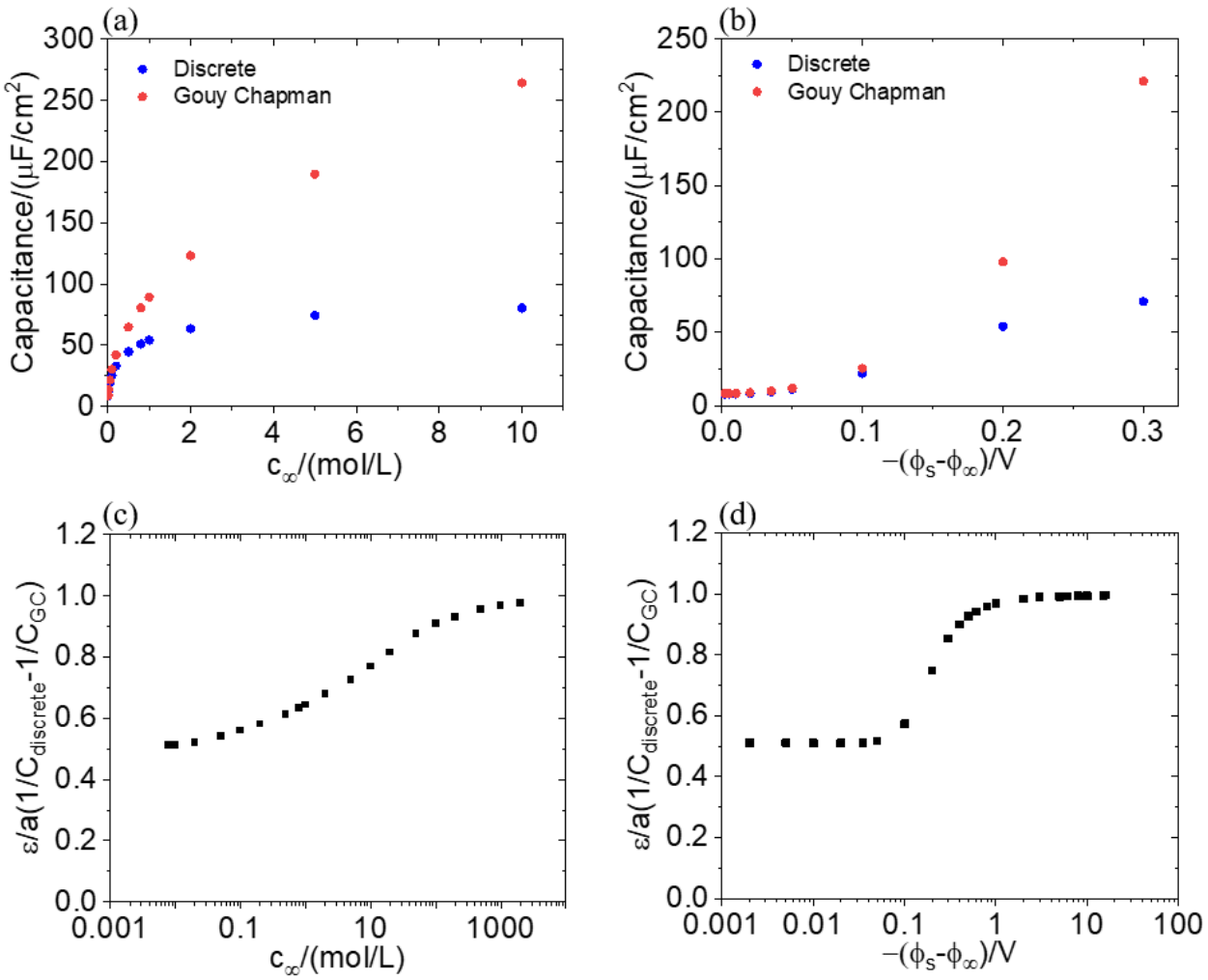

Figure S3. (a), (b) Calculated space charge capacitance of discrete model and Gouy Chapman model. (c), (d) Normalized Helmholtz corrections. (a), (c) potential on the metal surface is constant ($\phi_s - \phi_\infty$=-35 mV); (b), (d) bulk concentration is constant (c_∞=1 ×10^{-5} mol/cm^3). Helmholtz corrections are calculated by applying same total excess charge for both models. Simulation parameters: lattice spacing $\Delta x'$=0.1 nm; dielectric constant ε_r=10; μ^0 is constant; T=298 K.

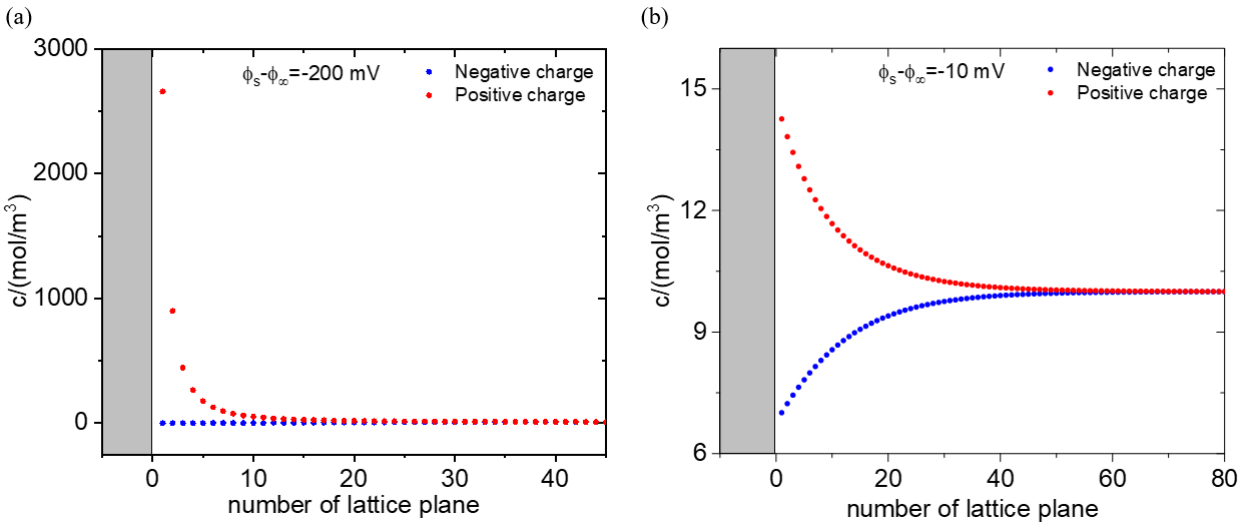

Figure S4. The profiles of charge carrier concentrations with different ϕ_s in discrete model. Simulation parameters: lattice spacing $\Delta x'$=0.1 nm; dielectric constant ε_r=10; c_∞=1 ×10^{-5} mol/cm^3; T=298 K; (a) $\phi_s - \phi_\infty$=-200 mV; (b) $\phi_s - \phi_\infty$=-10 mV. For large ϕ_s (a), only one carrier (positive charge in this example) is decisive. In the case of small ϕ_s (b), both positive and negative charge carriers are of importance.

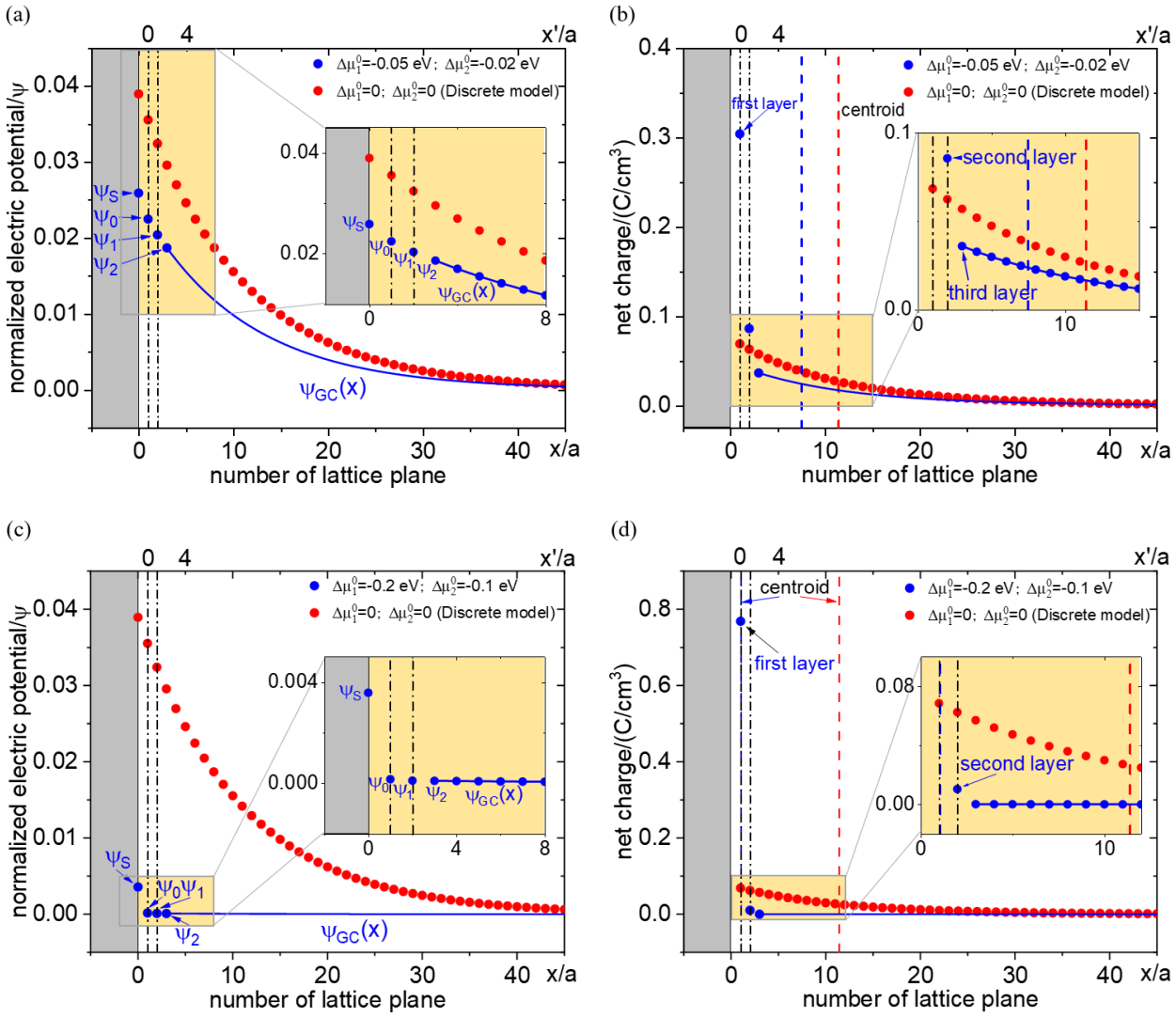

Figure S5. The profiles of (a), (c) electric potential and (b), (d) charge carrier concentration shown as a function of number of lattice plane. The blue data shows the model with μ^0-variation in the first two layers adjacent to the interface by $\Delta\mu_1^0$, $\Delta\mu_2^0$ with respect to the bulk. From third layer on the bulk value is applied. The blue curve shows the continuous model from third layer on. The red data shows the discrete model without μ^0-variation. Blue and red dashed lines in (b), (d) indicate the positions of centroid for both cases (with or without μ^0-variation). Black dash-dotted lines refer to the positions of first two layers. Simulation parameters: lattice spacing $\Delta x'$=0.1 nm; dielectric constant ε_r=10; $\phi_s - \phi_\infty$=-1 mV; $c_\infty = 1 \times 10^{-5}$ mol/cm^3; T=298 K; (a), (b) $\Delta\mu_1^0 = -0.05$ eV; $\Delta\mu_2^0 = -0.02$ eV. (c), (d) $\Delta\mu_1^0 = -0.2$ eV; $\Delta\mu_2^0 = -0.1$ eV.

Figure S6 displays discrete ϕ- and q- profiles for various conditions (constant surface potential or constant bulk concentration).

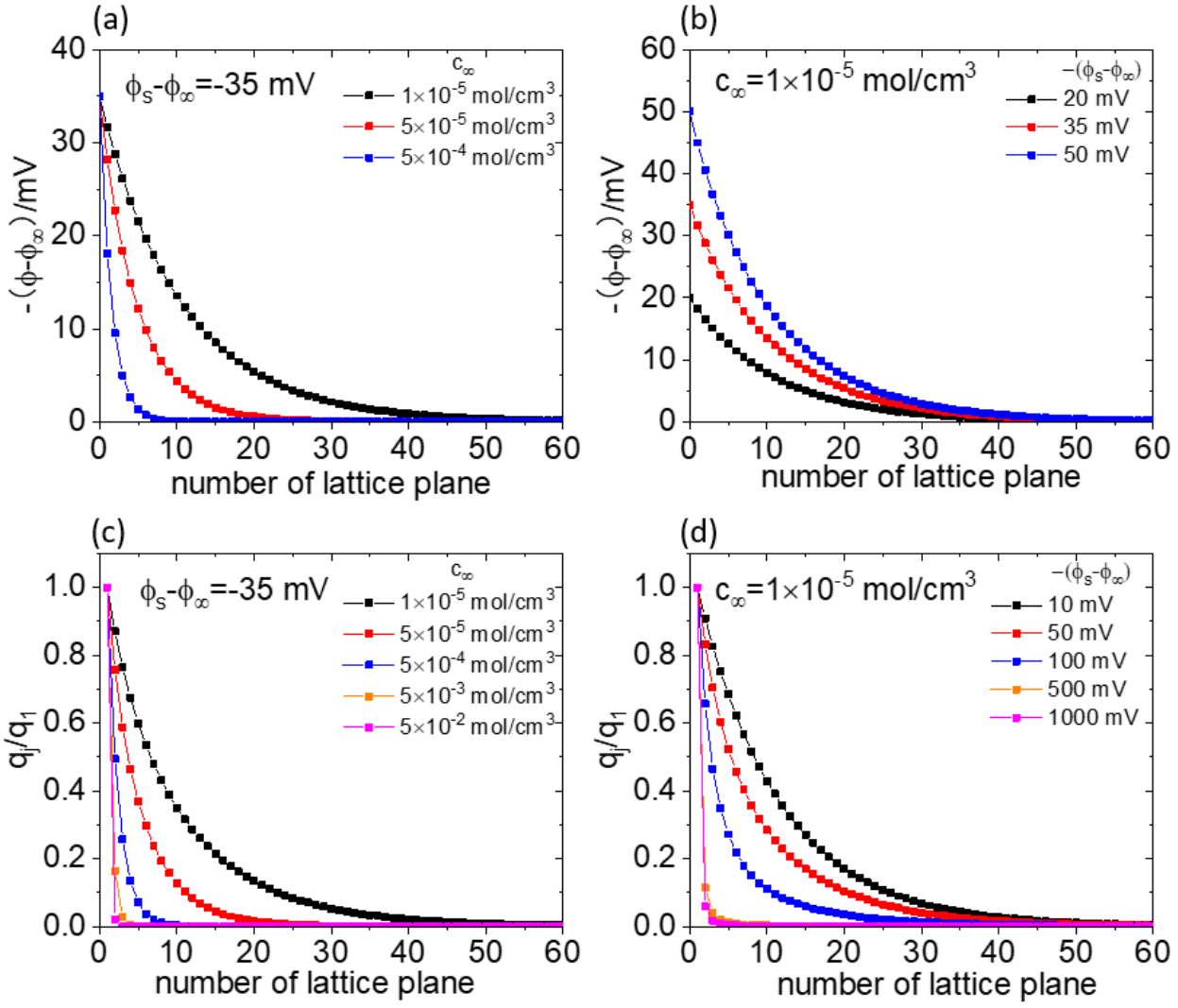

Figure S6 Profiles of (a), (b) electric potential and (c), (d) charge density normalized to the value at the first plane in discrete model shown as a function of number of lattice plane. Simulation parameters: lattice spacing $\Delta x'$=0.1 nm; dielectric constant ε_r=10; T=298 K. (a), (c) potential on the metal surface is constant ($\phi_s - \phi_\infty$=-35 mV); (b), (d) bulk concentration is constant (c_∞=1 ×10^{-5} mol/cm^3).

Table S1 (a) $\frac{\lambda}{a}$ = e

$\frac{b}{a}$	$\frac{\varepsilon}{b}\frac{1}{C}$	$\frac{\varepsilon}{b}\frac{1}{C}-\frac{\lambda}{b}$	$\frac{b-a/2}{b}$
2	2.1244	0.7653	0.7500
3	1.7496	0.8435	0.8333
4	1.5622	0.8826	0.8750
8	1.2811	0.9413	0.9375
16	1.1406	0.9707	0.9688

Table S1 (b) $\frac{\lambda}{a}$ = 5e

$\frac{b}{a}$	$\frac{\varepsilon}{b}\frac{1}{C}$	$\frac{\varepsilon}{b}\frac{1}{C}-\frac{\lambda}{b}$	$\frac{b-a/2}{b}$
2	7.5488	0.7531	0.7500
3	5.3658	0.8353	0.8333
4	4.2744	0.8765	0.8750
8	2.6372	0.9383	0.9375
16	1.8186	0.9691	0.9688

Table S2

ϕ_s	$\frac{Q_+}{Q_+ + Q_-}$
1 mV	0.50202
10 mV	0.52027
50 mV	0.6049
100 mV	0.71953
200 mV	0.88392
500 mV	0.97345
1000 mV	0.98935